



JP9955298

NATIONAL INSTITUTE FOR FUSION SCIENCE

**Polarization of Electron Cyclotron  
Emission Spectra in LHD**


P.C. de Vries, Y. Nagayama, K. Kawahata, S. Inagaki,  
H. Sasao and K. Nagasaki

(Received - June 8, 1999 )

NIFS-603

July 1999

**RESEARCH REPORT**  
NIFS Series

30 - 50 

NAGOYA, JAPAN

This report was prepared as a preprint of work performed as a collaboration research of the National Institute for Fusion Science (NIFS) of Japan. This document is intended for information only and for future publication in a journal after some rearrangements of its contents.

Inquiries about copyright and reproduction should be addressed to the Research Information Center, National Institute for Fusion Science, Oroshi-cho, Toki-shi, Gifu-ken 509-5292 Japan.

# Polarization of Electron Cyclotron Emission Spectra in LHD

P.C. de Vries<sup>1</sup>, Y. Nagayama<sup>1</sup>, K. Kawahata<sup>1</sup>, S. Inagaki<sup>1</sup>, H. Sasao<sup>1</sup> and K. Nagasaki<sup>2</sup>

<sup>1</sup>National Institute for Fusion Science, 322-6 Oroshi-cho, Toki-shi, 509-5292 Japan

<sup>2</sup>Institute of Advanced Energy, Kyoto University, Kyoto, 611-0011 Japan

Electron cyclotron emission (ECE) can be used to determine the electron temperature profile in magnetized plasmas. The complex structure of the magnetic field configuration in the Large Helical Device (LHD), which has a large shear, complicates the analysis of the ECE spectrum. In a sheared magnetic field the propagation of X and O-mode polarization through the plasma are coupled, causing mode conversion and polarization rotation. Mode scrambling is also caused by wall reflections. In this report, this mode conversion in LHD is numerically analyzed. It was found that at low density mode conversion scrambles the ECE spectra. However, at higher density ( $n_{e0} > 1.0 \cdot 10^{19} \text{ m}^{-3}$ ) the polarization mode is found to rotate with the sheared magnetic field, yielding only a negligible mode conversion. Wall reflections are found to depolarize the ECE spectrum. Notwithstanding the LHD magnetic configuration, it is shown that temperature profiles could be revealed from the ECE spectra.

**Keywords:** ECE emission / Mode conversion / Diagnostics

## I. Introduction

Electron Cyclotron Emission (ECE) spectroscopy has proven to be a powerful tool to measure temperature profiles in thermonuclear fusion plasmas<sup>1,2,3</sup>. The emission is generated by electrons, which gyrate around the magnetic field lines that confine the plasma, and is microwave range. The frequency is determined by the local magnetic field strength while the intensity is proportional to the temperature at the emission resonance. Because the plasma is a refractive medium for microwaves the waves may be interfered or re-absorbed before they reach the diagnostic antenna. Two polarization modes exists: X-mode if the electric field vector is perpendicular to the magnetic field and O-mode with a parallel electric field vector. The two polarization modes have different refractive indices and, hence, propagate differently through the plasma towards the diagnostic antenna.

In Tokamak plasmas, the analysis of ECE spectra is generally straightforward. The magnetic field is a monotonic decreasing function of the radius. Hence, different frequencies are emitted at different positions. Usually the second harmonic of the X-mode spectrum is monitored which is not interfered by cut-offs. More important is that this polarization mode is also optically thick for this harmonic. This means that plasma is a black body for these frequencies and the intensity is linearly proportional to the temperature at the resonance.

However, the situation is more complicated in the case of the Large Helical Device (LHD)<sup>4</sup>

( $R_0=3.75 \text{ m}$ ,  $a=0.6 - 0.9 \text{ m}$ ,  $B_0=1.5 - 3 \text{ T}$ ) which employs the so-called heliotron configuration with helical winding field coils around the plasma column. The magnetic field configuration is non-monotonous function of the radius; hence, equal frequencies are emitted at different positions in the plasma. The largest problem arises from the sheared field yielding a coupled propagation of X and O-mode. Mode conversion can take place along the propagation path. It may seem that it is more difficult to monitor a distinct polarization mode. Electron Cyclotron Heating (ECH) in heliotrons faces the same problem<sup>5</sup>. High power microwaves are launched into plasma and are absorbed at a local resonance. However, in a heliotron, mode conversion can take place. Because both modes have different absorption properties, part of the injected waves may not be absorbed if these effects are not taken into account.

Details of electron cyclotron emission from fusion devices, tokamaks in particular, have been reported in the past. In this report, the numerical analysis of ECE mode conversion in a heliotron will be presented. First the general effects of the sheared magnetic field on the propagation of coupled X and O-mode waves will be treated. The polarizing properties of the LHD plasma will be shown. Secondly, the multiple resonance's in the plasma will be discussed. Absorption and emission, which is different for the two polarization modes, is included in the

---

\* The magnetic shear is defined in this report as the field vector angular gradient in radial direction and not as the change in rotational transform.

calculations. In the complete report is assumed that absorption and emission only take place in a narrow region around the resonance's. Multiple resonance's may cause problems if one considers mode conversion. The X-mode wave, emitted at one resonance, is converted into O-mode and, hence, only partly absorbed by the second resonance. Besides the multiple resonance's, reflected waves from the wall opposite the diagnostic antenna, may scramble the spectrum. Part of the waves will be mode converted at reflection, which was also observed in earlier experiments<sup>6</sup>. Nevertheless, this scrambling of polarization modes is not important in tokamak experiments, because the plasma itself does not cause mode conversion, and X and O-mode can always be distinguished. In the last section, the applicability of ECE spectroscopy at LHD will be discussed. LHD is equipped with various ECE diagnostics<sup>7</sup> and first measurements of ECE spectra will be presented.

## II. Propagation of ECE waves in LHD

The analysis of ECE spectra is complicated in LHD because of its magnetic configuration. The diagnostic antenna collects radiation from the LHD equatorial plane and is located on the outside of the torus. The magnetic field profile, in the line-of-sight of the ECE diagnostic antenna, is shown in Fig. 1. It is a non-monotonic function of the major radius and has a maximum around  $R=3.6$  m. The diagnostic antenna is located at the outside of the torus. The central magnetic field value can be changed from  $B_{ax}=1.5$  T up to 3 T. The first setting, with  $B_{ax}=1.5$  T at  $R=3.6$  m, will be used in the numerical simulations shown in this report.

The frequencies emitted by the electrons are determined by the local magnetic field strength. Second harmonic frequencies, which are relevant for the determination of the temperature profile, are in the range of 50 GHz at the edge to 83 GHz in the center. Because of the non-monotonous magnetic field profile, equal frequencies are emitted from two different resonance layers. The first is directly viewed by the diagnostic antenna, while the second resonance is behind that. Emission from the second resonance might not be re-absorbed by the first one if the last is optically thin. Mode conversion can occur along the path between the two resonances, which also cause the second resonance emission to shine-through.

Propagation of ECE waves is determined by the refractive indices,  $N_x$ , and,  $N_o$ , for the two polarization modes. The refractive index is a

complex function of the wave frequency and plasma frequency, and therefore indirectly determined by the plasma density<sup>2</sup>. Normally the X and O-mode waves propagate independently towards the diagnostic antenna. However, in a heliotron the propagation is coupled. The coupling of X and O-mode propagation is caused by the large magnetic shear in LHD. In Fig. 1 the magnetic shear is given as the angle,  $\theta$ , between these to field components defined by:  $\tan\theta = B_z/B_p$ . The derivative of this shear is given by:  $\phi = d\theta/dr$ . In contrast to the tokamak configuration, where the magnetic shear is very small, the ratio between the poloidal and toroidal field component is of order unity in LHD.

Mode conversion can be illustrated by the example shown in Fig. 2. A wave propagates in vacuum in the  $r$ -direction from I towards II. The magnetic field is sheared along the  $r$ -axis. At I the wave has an electric field vector in the  $x$ -direction, while the magnetic field is perpendicular to that in the  $y$ -direction. It is an X-mode wave. In vacuum the wave polarization is not expected to change, hence, up to II the electric field vector remains in the  $x$ -direction. However, the magnetic field vector is rotated in the  $x$ - $y$  frame. The electric field vector has a component perpendicular (X-mode) and parallel (O-mode) to the magnetic field in II. Part of the X-mode power is converted into O-mode between I and II.

In dense plasmas the coupling of the two modes is described by their wave equations. *Fidone, et al.*<sup>8</sup> found for the propagation of X and O-mode waves along,  $r$ , perpendicular to the magnetic field the following second order coupled equations:

$$\frac{d^2 E_{||}}{dr^2} + \left(\frac{\omega^2}{c^2} N_x^2 - \phi^2\right) E_{||} = +2\phi \frac{dE_{\perp}}{dr} + E_{\perp} \frac{d\phi}{dr}, \quad (1a)$$

$$\frac{d^2 E_{\perp}}{dr^2} + \left(\frac{\omega^2}{c^2} N_o^2 - \phi^2\right) E_{\perp} = -2\phi \frac{dE_{||}}{dr} - E_{||} \frac{d\phi}{dr}, \quad (1b)$$

where,  $\theta$ , and,  $\phi$ , are defined above and the  $E_{\perp}$  and  $E_{||}$  are the electric field components of the X and O-mode, respectively. If the shear is negligible ( $\phi=0$ ) one obtains two uncoupled wave equations and the two modes will propagate independently.

If the refractive indices are equal for both modes, for example in vacuum, mode conversion takes place. The electric field vector has the inertia to preserve its polarization, however,  $E_{\perp}$

and  $E_{\theta}$  change *mode conversion*. If the refractive indices differ, both modes do not propagate independently, yielding Faraday rotation. The polarization of the electric field vector will rotate with the magnetic field; i.e. *polarization rotation*. Furthermore, the different propagation velocities of X- and O-mode may cause an *elliptization* of linear polarized waves. It is possible to calculate the amount of mode conversion and polarization rotation in specific plasma by solving numerically the two coupled differential equations.

The three effects on wave propagation, addressed above, will be discussed. The density and temperature profiles are assumed to be simple functions of the minor radius with a maximum at  $R=3.75$  m. The temperature profile is taken to be parabolic ( $l=2$ ), while the density profile is squared parabolic ( $m=4$ ):

$$T_e(r) = T_{eo} \left( 1 - \left( \frac{r}{a} \right)^l \right) \quad n_e(r) = n_{eo} \left( 1 - \left( \frac{r}{a} \right)^m \right) \quad (2)$$

Density profiles are observed to be flat in heliotron devices. The magnetic field configuration as shown in Fig. 1 is used.

An X-mode microwave emitted in the plasma center with a second harmonic frequency of  $f=81$  GHz propagates towards the outside along the  $r$ -axis while the magnetic field is sheared in the  $x$ - $y$  plane. On the magnetic axis, the magnetic field is parallel to the  $y$ -axis and perpendicular to the  $x$ -axis. The coupled wave equations are numerically solved using Adams-method. X-mode emission means that the initial electric field vector of the wave is perpendicular to the local magnetic field, i.e. in  $y$ -direction at  $R=3.6$  m. O-mode emission is assumed to be zero and absorption is neglected for now.

First the propagation in vacuum ( $N_x = N_o = 1$ ) will be treated. In Fig. 3a the power fraction ( $\propto E^2$ ) of the X and O-mode are shown as a function of radius. The initial X-mode wave is slowly converted into O-mode during propagation. The electric field components in  $x$  and  $y$  direction are not changed. The initial direction of polarization ( $y$ -direction) does not change in vacuum. The wave travels in vacuum with a constant polarization, however, the projections on the magnetic field (X and O-mode) change due to the magnetic field shear. The power fractions of X and O-mode plotted in Fig. 3a are therefore equal to  $P_x = E^2 \cos^2 \theta$  and  $P_o = E^2 \sin^2 \theta$ .

The situation is different in dense plasmas. In Fig. 3b the X and O-mode power fractions are shown for a wave which propagates through the

plasma with a density profile:  $n_{eo} = 3.0 \cdot 10^{19} \text{ m}^{-3}$ ,  $m=4$ . In this high density case, when  $N_x < N_o$ , the X-mode power remains constant up to the edge of the plasma ( $r=0.9$  m). In the vacuum region ( $r>0.9$  m), again a conversion from X to O-mode is observed. Inside dense plasmas, the wave remains its polarization with respect to the local magnetic field vector. Because it is sheared, the power fractions in  $x$  and  $y$ -direction vary, as shown in Fig.3b. A rotation of polarization occurs in the laboratory ( $x$ - $y$ ) frame at high density. In all cases, the elliptization of the initial linearly polarized X-mode wave was found negligible. Elliptization will play a role in the mode scrambling if the emitted O and X-mode have the same order of magnitude, and if a fixed initial phase relation exist. If microwaves, with a specific polarization, are send into the plasma, for example for purpose of ECH, this will be the case. However, no specific phase between X and O-mode waves emitted by the plasma. Elliptization effects are therefor found to average out for ECE.

Polarization rotation depends strongly on the density. In Fig. 4 the polarization angle is shown for several densities (assuming again typical profiles with  $m=4$ ). The polarization angle is defined as the angle of polarization within the laboratory  $x$ - $y$  frame at  $r=a$ .

It is found that in vacuum, the polarization angle is unchanged in the  $x$ - $y$  frame, i.e. the each frequency has a polarization angle given by the angle of the local magnetic field where it is emitted. The calculation for  $n_{eo} = 0.25 \cdot 10^{19} \text{ m}^{-3}$  shows that the lower frequencies, emitted in the outer plasma region, are still not due to polarization rotation. While at higher frequencies the polarization angle starts to deviate from the initial angle in the  $x$ - $y$  frame. For densities larger than  $n_{eo} > 1.0 \cdot 10^{19} \text{ m}^{-3}$  polarization rotates almost up to the edge of the plasma. Hence, all frequencies exit the plasma under approximately the same angle. For the high-density case ( $n_{eo} = 3.0 \cdot 10^{19} \text{ m}^{-3}$ ) the polarization angle of the ECE X-mode emission approaches  $35^\circ$ , which is perpendicular (X-mode) to the magnetic field at  $r=a=0.9$ m.

### III. Effect of multiple resonance's and reflections

Polarization rotation can be favorable with respect to reflections and the double resonance layer in a heliotron device. In high-density plasmas, the wave will remain its polarization. Hence, X-mode waves emitted at the inner ECE resonance will be absorbed at the outer resonance if it is optically thick. Furthermore, effect of reflections from the back wall will also be reduced in the optically thick, high density, plasma. In this section, absorption and emission are included in the calculations.

Emitted waves propagating can be refracted or re-absorbed. The absorption, emission and refraction is different for the two polarization components<sup>2,3</sup>. If the density is high enough, second harmonic X-mode waves will be interfered by the upper cut-off, while the O-mode component of the wave can pass freely. For  $B_o=1.5$  and  $B_o=3$  T this occurs at  $n_{eo}>3\cdot 10^{19} m^{-3}$  and  $n_{eo}>13\cdot 10^{19} m^{-3}$ , respectively. The O-mode is shielded by the plasma frequency resonance for at  $n_{eo}>6.7\cdot 10^{19} m^{-3}$  for  $B_o=1.5$  T. Usually, The upper cut-off will shield the lower frequencies emitted at the edge first, because of the flat density profiles in LHD. Higher densities are required in order to affect ECE emitted at the center.

The relation between the intensity of the ECE emission and black body temperature is determined by the optical depth,  $\tau$ , which is the integrated absorption along the propagation path<sup>2</sup>. If the plasma is optically thick (i.e. it has a large optical depth for a specific frequency and polarization mode); the intensity of this frequency component is linearly proportional to the local temperature. Furthermore, equal frequencies will be completely re-absorbed.

The absorption coefficients for each harmonic resonance and polarization mode have been calculated for finite plasma density<sup>3</sup>. Common expressions for the optical depth in tokamak plasmas can be derived from this, however these cannot be applied to heliotrons. This is because they assume that the resonance width is narrow in both frequency and radial space<sup>2</sup> (i.e.  $d\omega/dR$  is finite). This is not valid in the center of a heliotron, hence, proper integration is required. Integration of the absorption coefficient for the second harmonic frequencies in LHD showed that the X-mode is largely optically thick for  $n_{eo}>1.5\cdot 10^{19} m^{-3}$  and  $B_o=1.5$  T. With the  $B_o=3$  T magnetic configuration higher densities will be required

( $n_{eo}>2\cdot 10^{19} m^{-3}$ ). Nevertheless, at low densities one should be aware of an optical gray area at the edge of the plasma. The optical depth of second harmonic O-mode is normally lower by a factor  $kT/m_e c^2$ . It can be concluded that second harmonic O-mode emission will be very low in LHD at low temperature (i.e.  $T_{eo} < 3keV$ ). O-mode waves, emitted by the plasma, or caused by mode conversion will hardly be re-absorbed at a resonance.

The shine-through and re-absorption of ECE emitted from the second resonance has been calculated. An X-mode wave, emitted at the inside resonance, propagates towards the antenna and encounters the outside resonance. The emission resonance is chosen to be at,  $r=-0.7$  m and the outside resonance was found at  $r=+0.42$  m. The mode conversion along the propagation path is calculated accordingly. The powers of X and O-mode are reduced inside the resonance, by a factor of,  $e^{-\tau}$ , where  $\tau$  is the resonance's optical depth for the two polarization modes, respectively.

Two examples for different densities are shown in Fig. 5a-b. At very low density ( $n_{eo}=0.25\cdot 10^{19} m^{-3}$ ), the optical depth of the outside resonance for the X-mode is low. X-mode power shines through and is able to reach the antenna. Furthermore, part of the X-mode power is mode converted in the low-density region at the edge. However, as also found in the previous section, even at this low density, minor mode conversion is found in the central part. In Fig. 5b it is shown that mode conversion is negligible at the density of  $n_{eo}=1.0\cdot 10^{19} m^{-3}$ . The emitted X-mode is almost completely re-absorbed at the outside resonance. A shine-through level less than 5% was found. The shine-through fraction for all second harmonic frequencies, emitted at the inside resonance, is shown in Fig. 5c, for three different density profiles. The mode conversion fraction, the ratio between the original X-mode power and the O-mode power at the edge, was always smaller than 7% for  $n_{eo}>0.25\cdot 10^{19} m^{-3}$ . A strong shine-through component is found due to small re-absorption at the outside resonance. If the density is  $n_{eo}>1\cdot 10^{19} m^{-3}$  a maximum shine-through fraction of 10% is found for edge frequencies, but this decreases with increasing optical depth for higher densities.

ECE spectroscopy measurements are irrelevant at densities lower than  $n_{eo}<1.0\cdot 10^{19} m^{-3}$ , due to the required optical thickness. Mode conversion is negligible in the relevant high-density cases. Therefore, we assume that X and O-mode propagate independently through the LHD plasma, while rotating with the sheared magnetic field in the x-y frame. This makes it easier to

handle the calculations of shine-through emission and reflected waves. The only difference with the situation in tokamaks, is the presence of a second resonance in the line-of-sight of the diagnostic antenna. One outside resonance in front of the antenna and an inside resonance behind that. The intensity of a spectral component, with a frequency,  $\omega$ , can be determined. If the temperatures at resonance's of this frequency are,  $T^{out}$ , and,  $T^{in}$ , respectively, one find:

$$T^{rad}(\omega) = T^{out}(1 - e^{-\tau^{out}}) \frac{1 - \rho e^{-\tau^{out}} e^{-\tau^{in}} + \rho e^{-\tau^{out}} e^{-2\tau^{in}}}{1 - \rho e^{-\tau^{out}} e^{-\tau^{in}}} + T^{in}(1 - e^{-\tau^{in}}) e^{-\tau^{out}} \frac{1 - \rho e^{-\tau^{out}} e^{-\tau^{in}} + \rho e^{-\tau^{in}}}{1 - \rho e^{-\tau^{out}} e^{-\tau^{in}}}, \quad (3)$$

Where,  $\rho$ , is the reflectivity of the wall opposite of the antenna. Usually the reflectivity is about  $\rho = 90\%$  for a stainless steel wall. This expression gives the intensity, including that from multiple reflections between the vacuum vessel walls. The optical depth,  $\tau$ , of the two resonance's, gives the amount of re-absorption and the intensity of the emission. The integrated absorption through the plasma is:  $e^{-\tau^{in}} e^{-\tau^{out}}$ . This equation differs from that of tokamaks, however, if one assumes one resonance to be optically thin, the usual one resonance, tokamak, expression is obtained.

If the outside layer is optically thick, the second term at the right-hand-side, can be neglected, i.e. emission of the inside layer is completely re-absorbed. Reflected waves are also re-absorbed and, as usual, the first term, becomes only dependent on the temperature:  $T^{rad} = T^{out}$ . Hence, in the case of an optically thick outside resonance, the spectral intensity depends on the temperature at this resonance. At high density  $n_{e0} > 1.0 \cdot 10^{19} \text{ m}^{-3}$  this is the case for second harmonic X-mode in LHD. However, if the resonance layers are not optically thick, for example at low density in the plasma edge, or for O-mode, the intensity is determined by the temperatures at both resonances. Hence, the measurement is not localized and it will be difficult to determine a temperature profile.

Of course, one should mind that the X and O-mode exit the plasma under an angle, as shown in the previous section. Furthermore, reflections can still scramble the spectrum, even if the resonance is optically thick. This is due to the mode conversion caused at reflection. Though only very small,  $\pi \approx 10\%$ , multiple reflections can largely increase the mode converted reflected

intensity. This effect has been reported already in the first ECE measurements from tokamaks, where it was found to de-polarize the spectrum<sup>6</sup>. If it is assumed that the emission of O-mode ECE at the two resonance's is very low, i.e. O-mode is optically thin, All detected O-mode is due to mode converted reflections. In LHD the optical thickness of second harmonic O-mode is found negligible for moderate densities between and temperatures below  $T < 3 \text{ keV}$ . Under this assumption the mode-converted fraction is given by<sup>6</sup>:

$$T^{MC}(\omega) = \frac{\pi \rho^e}{1 - \rho^e + \pi \rho^e} \left\{ T^{in} (1 - e^{-\tau^{in}}) + T^{out} e^{-\tau^{in}} (1 - e^{-\tau^{out}}) \right\} \quad (3)$$

$$\quad (4)$$

The effective reflectivity  $\rho^e$  of one polarization mode is less than that given by  $\rho$  because part returns in a different mode. Therefore, the reflectivity,  $\rho$ , in Eq. (3) should be replaced by the effective reflection coefficient given by:

$$\rho^e = \rho \left\{ 1 - \frac{\pi(1-\rho)}{1-\rho+\pi\rho} \right\}. \quad (5)$$

Hence, it is easy to calculate that with,  $\pi=0.1$  and  $\rho=0.9$ , that the mode converted reflections have an intensity which is about 50% of the X-mode intensity. For larger reflectivity, the polarization component perpendicular to X-mode increases. In the above equation, it is assumed that the emission originates from within the narrow antenna pattern. However, the vessel wall may focus reflected waves into the antenna, from a much larger part of the plasma. The reflected intensity is thus expected to be larger, than found from eq. 4. Even if the plasma does not emit O-mode ECE, a strong O-mode component is detected. Reflections of X-mode are re-absorbed at high density and cannot enter the diagnostics.

#### IV. Temperature profiles by ECE spectroscopy

In the previous sections, the effects of mode conversion and multiple resonance's on the ECE spectrum have been shown. It was found that the polarization of the ECE spectrum would be mainly influenced by reflections while at higher density polarization rotation prevented mode

conversion inside the plasma. In this section, the intensity of the spectral O-mode and X-mode component will be calculated.

It has been assumed that the emission originated from two narrow resonances with different emission and absorption properties for X and O-mode. The equations given in the previous section have assumed O-mode emission and absorption to be zero. As the wave's pass one of the resonances, the intensity of the two modes is reduced according to the local absorption. Part of the wave will be reflected at the wall. Furthermore, the reflection causes a small mode conversion. The reflection coefficient and mode conversion fraction are taken to be,  $\rho=0.9$  and  $\pi=0.1$ , respectively. It has been assumed that mode conversion is negligible if only densities of  $n_{eo}>1.0\cdot 10^{19} m^{-3}$  are used. The X and O-mode defined as the polarization component perpendicular and parallel to the magnetic field at  $r=a$ , respectively. The intensity for all second harmonic frequencies is determined.

In Fig. 6 an example is shown for a moderate density of  $n_{eo}=1.0\cdot 10^{19} m^{-3}$  and a temperature,  $T_{eo}=1 keV$  (with profiles,  $m=4$  and  $l=2$ ). The temperature profile is shown, as a function of the frequency of the outside resonance. The X-mode power is nicely proportional to these temperatures. Only a small deviation at the edge is observed due to insufficient optical depth. However, at higher densities this optical gray area decreases. A large O-mode intensity is found which is predominantly due to mode converted reflections. O-mode emission at these low temperatures in LHD is negligible.

Usually ECE diagnostics measure only one polarization component. Because the two modes have an angle with respect to the laboratory  $x$ - $y$  frame, the measured intensity in the  $x$ -direction is not identical to the X-mode power. In Fig. 6, the power measured in the  $x$ -direction is shown. It is a mix between X and O-mode. The power of the wave component with an angle  $\alpha$  with the  $x$ -axis is given as,

$$T(\alpha) = T^x \cos^2(\alpha - \theta(a)) + T^o \sin^2(\alpha - \theta(a)), \quad (6)$$

where,  $\theta(a)$ , is the angle of the magnetic field within the laboratory frame at  $r=a$ .

At LHD, it is possible to choose the polarization direction of the detected radiation that is fed to the ECE diagnostics. A polarization rotator is installed for this purpose in the circular waveguide system<sup>7</sup>. This polarization rotator is able to select only the X-mode component by

setting the appropriate angle with respect to the  $x$ - $y$  frame. If a different angle is set, a different mix of O and X-mode is detected.

In Fig. 7a the ratio between the measured power,  $T(\alpha)$ , and the temperature at the outside resonance is shown, for all spectral components. If the polarization rotator is aligned ( $\alpha=\theta(a)=35^\circ$ ) to the magnetic field at  $r=a$ , the central frequencies are proportional to the local temperature. Only in the optical gray edge region, large deviations are found. At higher densities more frequencies become optically thick, as shown in Fig. 7b. Only a fraction of the temperature is measured if the polarization rotator is set differently. Pure O-mode is detected under an angle of ( $\alpha=\theta(a)+90=125^\circ$ ).

Hence, even in the presence of two resonance's and with the effect of mode converted reflections it will be possible to reveal the local temperature at the (outside) resonance viewed by the antenna. The polarization rotator should be set to the appropriate angle. From Eq. (4) it can be shown, that if the inside resonance is also optically thick, the O-mode intensity is linearly proportional to the local temperature at this resonance. This might be a possibility to deduce information from the other side of the magnetic field profile.

## V. Discussion

At LHD second harmonic ECE is monitored in order to deduce a temperature profile. The requirement is a sufficient high density. It was shown that the second harmonic X-mode is optically thick and that mode scrambling inside the plasma is negligible at  $n_{eo}>1.0\cdot 10^{19} m^{-3}$  for  $B_{ax}=1.5 T$  or  $n_{eo}>1.5\cdot 10^{19} m^{-3}$  for  $B_{ax}=3.0 T$ . However, at low density one should mind optical gray areas. At  $n_{eo}=1.0\cdot 10^{19} m^{-3}$  and  $m=4$  a maximum fraction of 10% was found to shine-through from the inner resonance which increases the observed intensity.

Wave propagation in a sheared magnetic field has been numerically analyzed. It was assumed that reflected waves and emission from the inside and outside resonance's did not affect each other. A difference between calculations for ECE waves or those used for ECH, is that in the later case a definite phase relation between X and O-mode exist, for example a linear polarized wave is injected. In that case, the initial X and O mode wave are in phase. For microwaves emitted by the plasma, no such a relation exist, hence the results are averaged over all possible phases or polarization possibilities. Because, the O-mode



level is very low for low LHD temperature plasmas, usually the above is not important. The initial emitted wave is entirely X-mode.

Inside the plasma, mode conversion was found negligible if the waves propagated through a sufficient high density ( $n_{eo} > 1.0 \cdot 10^{19} \text{ m}^{-3}$ ). Calculations for a magnetic field of  $B = 1.5 \text{ T}$  have been shown. The results did not differ for higher magnetic fields. Although the refractive indices of the two polarization modes are slightly different, the mode conversion properties depend mainly on the shear of the field and not the absolute strength of the field.

The polarization modes were found to rotate with the magnetic field almost up to the edge of the plasma. Mode conversion can also be caused by reflections. At high density, the X-mode polarization of the reflected waves is re-absorbed inside the plasma. Hence, they do not affect the measurement. However, mode converted reflections of the X-mode are not, because of the plasma is optical thin for O-mode. The O-mode emission will be small at moderate densities and temperature ( $T < 3 \text{ keV}$ ), while the dominant contribution is to the measured O-mode from the plasma is due to mode converted reflections of X-mode emission.

For the reconstruction of the temperature profile, only the second harmonic X-mode component of the ECE from the resonance viewed by the antenna should be detected. Otherwise, O-mode emission and reflected mode converted X-mode will scramble the measurement. To do so, a polarization rotator should be aligned with the magnetic field vector at  $r = a$ . The required polarization mode is expected to exit the plasma perpendicular to this. After this, the specific polarization of the ECE is fed to the spectroscopic diagnostics.

A fixed angle is chosen for the polarization rotator. However, small deviation might occur in the angle at which the X-mode is emitted by the plasma. Firstly, it can be observed in Fig.4 that the polarization angle is not equal for all frequencies. Furthermore, it varies with the density. A maximum variation of  $6^\circ$  is found for densities above  $n_{eo} > 1.0 \cdot 10^{19} \text{ m}^{-3}$ . Secondly, the position of the plasma edge may be different. The minor radius, which was chosen to be  $a = 0.9 \text{ m}$  in this report but the angle of the magnetic field at the edge will be smaller with decreasing  $r = a$ . The shift of the plasma position will have a similar effect. Variations of the polarization angle due to changes in the plasma edge position were estimated to be approximately  $5^\circ$ . Furthermore, deviations of the magnetic field configuration will be caused by, for example the bootstrap current, at high  $\beta$ . A measurement error

of  $\Delta\beta = \pm 5^\circ$  yields an error in the measurement of the X-mode power of to  $\cos^2\Delta\beta \approx 3\%$ . This is still smaller than the error made in the calibration of the diagnostics, which is approximately  $10\%$ . Therefore, major corrections are only required in the case of large modification in the magnetic field configuration.

At LHD, three different spectroscopic techniques are applied to measure the ECE spectrum. It is possible to monitor opposite polarization mode simultaneously. Up to now, the ECE diagnostics have been cross-calibrated against temperature profiles, measured by the Thomson-scattering diagnostic. It should be noted that in this case, the observed intensity is mostly found to be proportional to the temperature at the outside resonance. Even if the polarization rotator is set differently and a mix of O and X-mode is detected. In Fig. 7 it can be seen that the intensity of the spectrum is always more or less proportional to the temperature, for each polarization rotator setting. This is mainly because the temperature and magnetic field profiles are almost symmetric around the plasma axis.

The polarization of the ECE spectrum can be observed by changing the polarization rotator setting on a shot-to-shot base. Identical discharges, with sufficient high density are compared. The peak intensity of the ECE spectrum, measured by the Michelson Interferometer<sup>7</sup>, is shown in Fig. 8 as a function of the polarization rotator setting. A  $\cos^2$ -function is recognized, as expected from Eq. (6), can be seen.

Future experiments will be dedicated to a more accurate measurement of the spectral polarization. Simultaneous measurements of X and O-mode will be performed in the next experimental cycle of LHD.

## Acknowledgement

The work presented in this paper has been performed with financial support of the Japan Society of Promotion of Science and the National Institute for Fusion Science.

## References

---

- <sup>1</sup> A.E. Costley, in the Proc. of the Course on *Diagnostics for Fusion Reactor Conditions*, Varenna Italy (1982).
- <sup>2</sup> I. H. Hutchinson, *Principles of Plasma Diagnostics* Cambridge Univ. Press (1987).
- <sup>3</sup> M. Bornatici, *et al.*, Nucl. Fusion **23** (1983) 1153.
- <sup>4</sup> M. Fujiwara, *et al.*, J. Fusion Energy **15** (1996) 7.
- <sup>5</sup> K. Nagasaki, *et al.*, Plasma Phys. **6** (1999) 556.
- <sup>6</sup> A.E. Costley, *et al.*, Phys. Rev. Lett. **33** (1974) 758.
- <sup>7</sup> Y. Nagayama, *et al.*, Rev. Sci. Instrum. **70** (1999) 1034.
- <sup>8</sup> I. Fidone and G. Granata, Nucl. Fusion **11** (1971)133.

## List of Figures

Fig. 1: Magnetic field configuration at the ECE diagnostics cross section for  $B_{ax}=1.5 T$  and  $R_{ax}=3.6 m$

Fig. 2: Example of mode conversion in a sheared magnetic field.

Fig. 3: a) Normalized amplitude of the O and X-mode powers for a wave propagating in LHD in vacuum. Additionally the power fractions in, respectively,  $x$  and  $y$ -direction are given. b) Similar calculation but now for a dense plasma with  $n_{eo}=3.0 \cdot 10^{19} m^{-3}$   $m=4$ . The sum of the two electric field components is not constant along the propagation path because the total power of the wave in a refractive plasma is determined by:  $E \times B = N_x E_x^2 + N_o E_o^2$ . Because the refractive indices are below unity, the wave vector amplitude will decrease with density.

Fig. 4: The calculated polarization angles of linear polarized waves emitted in X-mode are shown for density profiles with  $n_{eo}=0, 0.25, 1.0, 3.0 \cdot 10^{19} m^{-3}$  (diamonds, triangles, open and closed circles respectively). The higher frequencies are emitted in the plasma center. The polarization angle is defined as the angle which the wave electric field vector has with respect to the  $x$ -axis at  $r=a$ .

Fig. 5: Calculated shine-through of a X-mode wave emitted at a resonance at  $r=-0.7 m$ . Part of the X and O-mode power is re-absorbed at the outside resonance at  $r=0.42 m$ . Two cases are shown: a)  $n_{eo}=0.25 \cdot 10^{19} m^{-3}$  b)  $n_{eo}=1.0 \cdot 10^{19} m^{-3}$ . c) The shine-through fraction for all frequencies, calculated for  $n_{eo}=0.25, 1.00, 3.00 \cdot 10^{19} m^{-3}$  and  $m=4$ . The corresponding mode conversion fraction is given by the dashed lines.

Fig. 6: Second harmonic ECE spectrum, calculated for  $n_{eo}=1.0 \cdot 10^{19} m^{-3}$  and,  $T_{eo}=1 keV$  ( $m=4$  and  $l=2$ ) and  $B=1.5 T$ . The O and X-mode components, at  $r=a$ , are given by the triangles and circles, respectively. The power in the  $x$ -direction is indicated by the diamond line, while the temperature at the outside resonance is shown by the fat line.

Fig. 7: The fraction of the measured power and the temperature at the outside resonance, given for different polarization rotator settings. a)  $n_{eo}=1.0 \cdot 10^{19} m^{-3}$  and  $T_{eo}=1 keV$  ( $m=4$  and  $l=2$ ) b)  $n_{eo}=2.5 \cdot 10^{19} m^{-3}$  and  $T_{eo}=1 keV$  ( $m=4$  and  $l=2$ )

Fig. 8: ECE intensity measured with the Michelson Interferometer for various rotator angles.

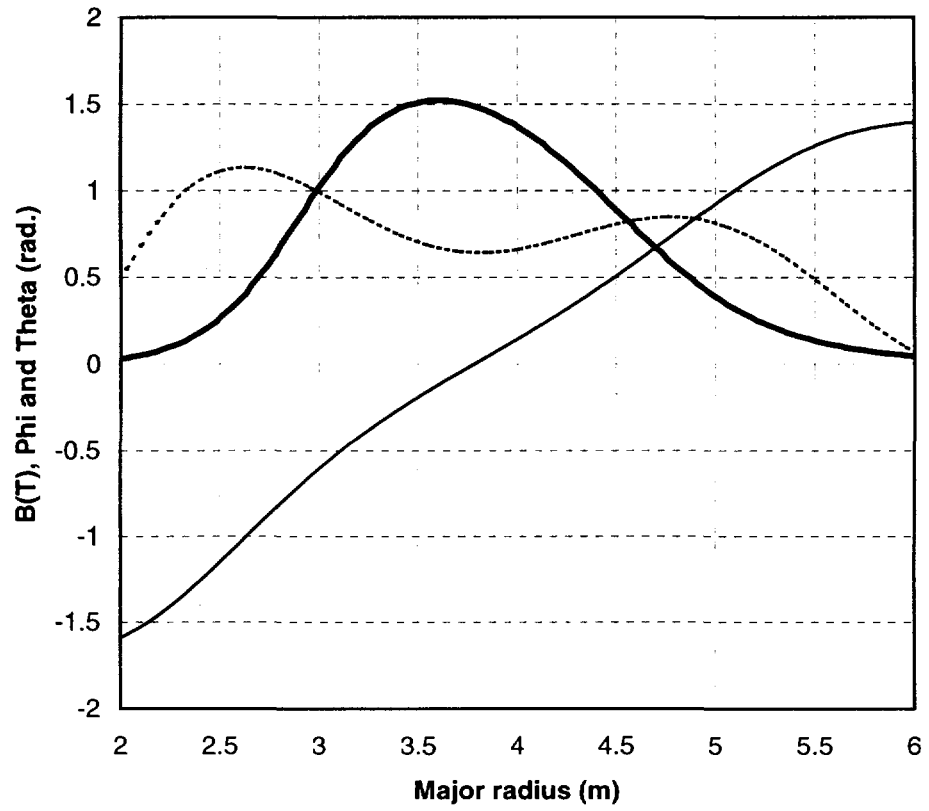


Figure 1

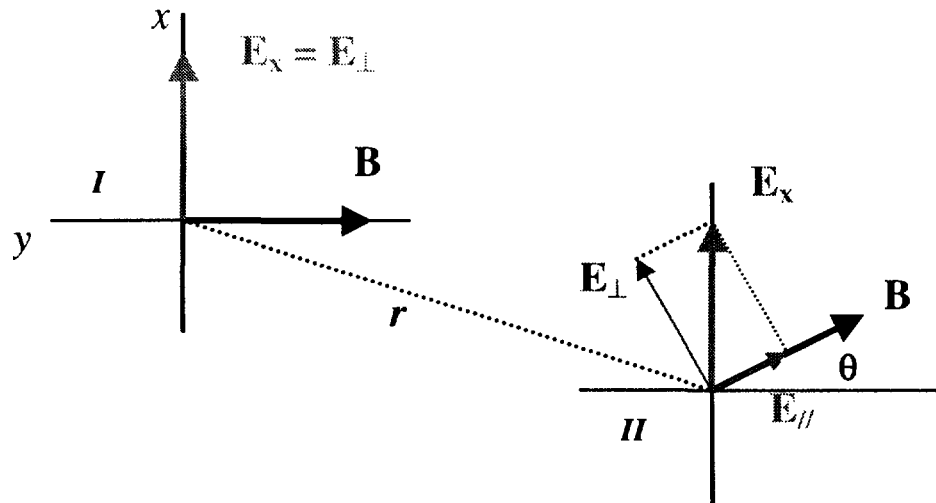


Figure 2

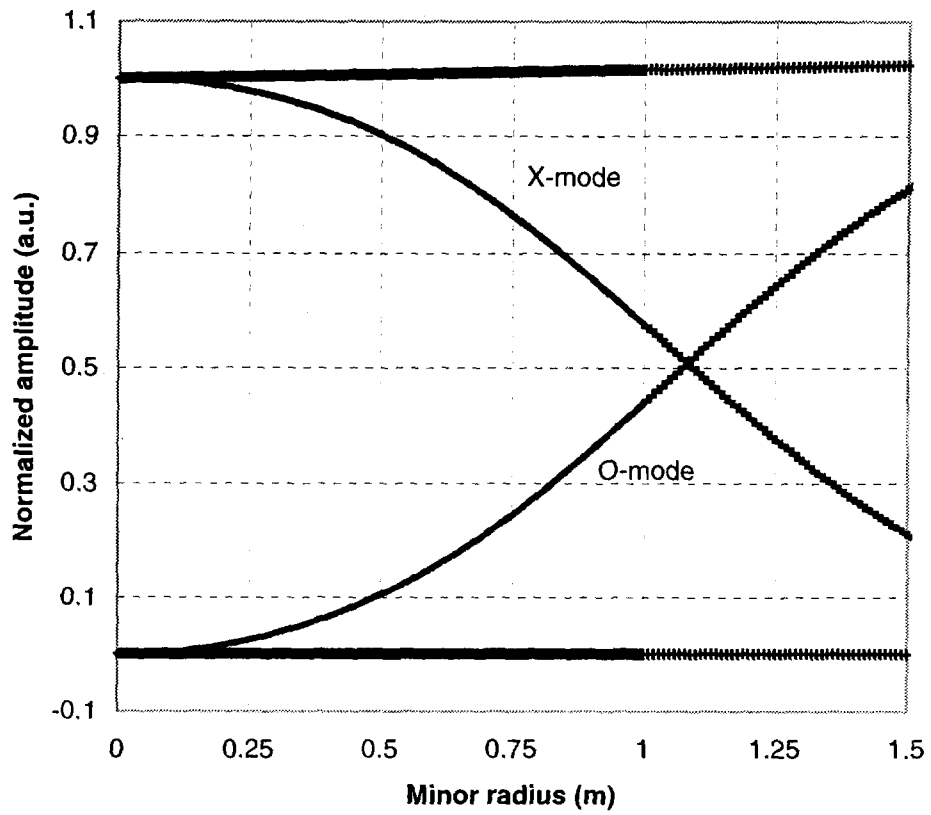


Figure 3a

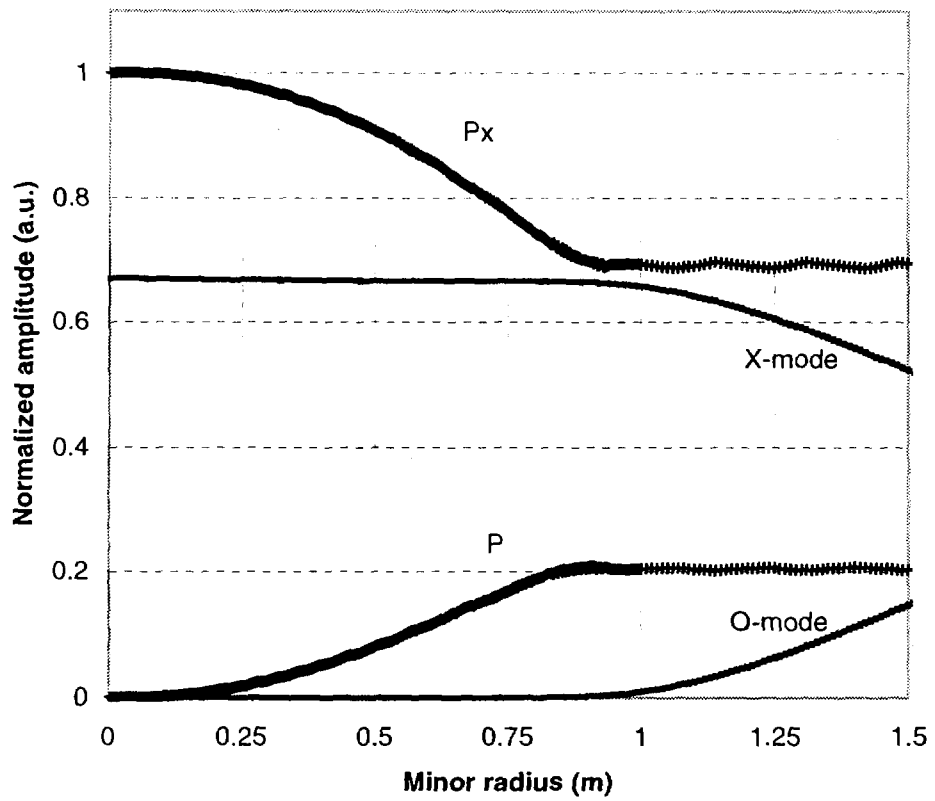


Figure 3b

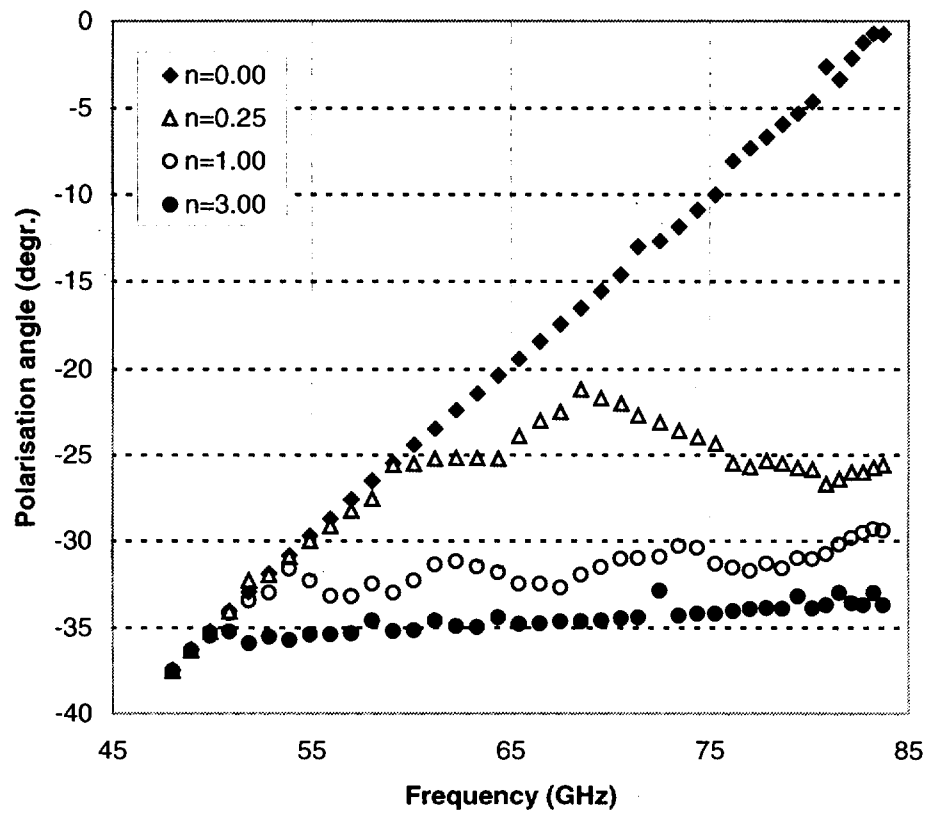


Figure 4

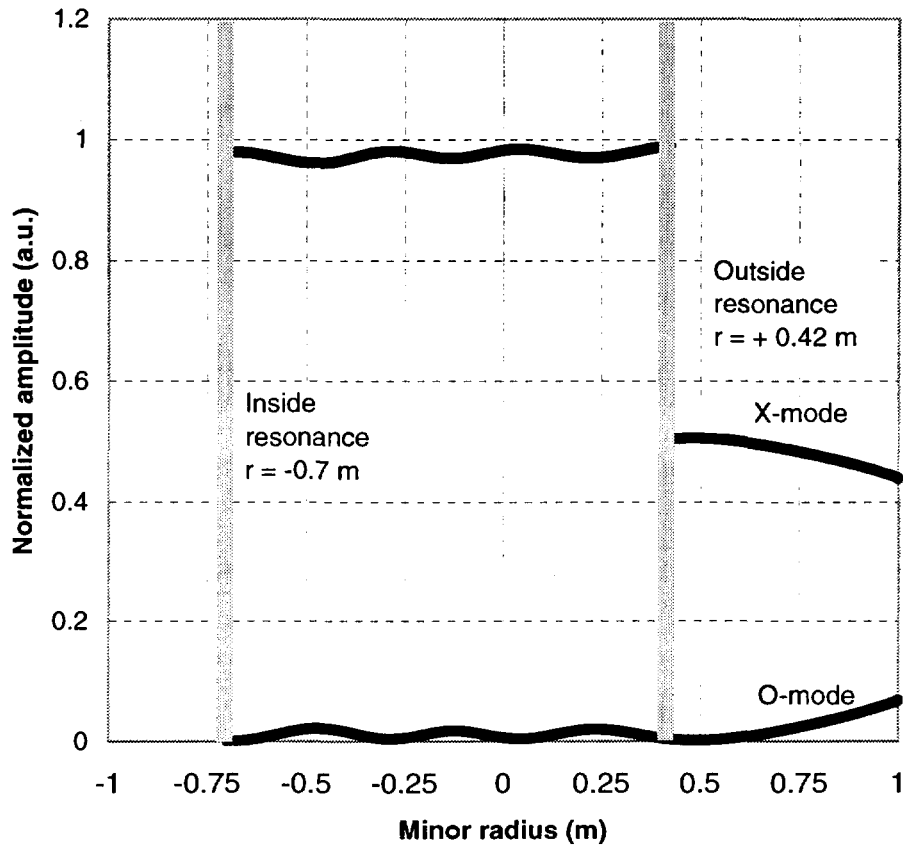


Figure 5a

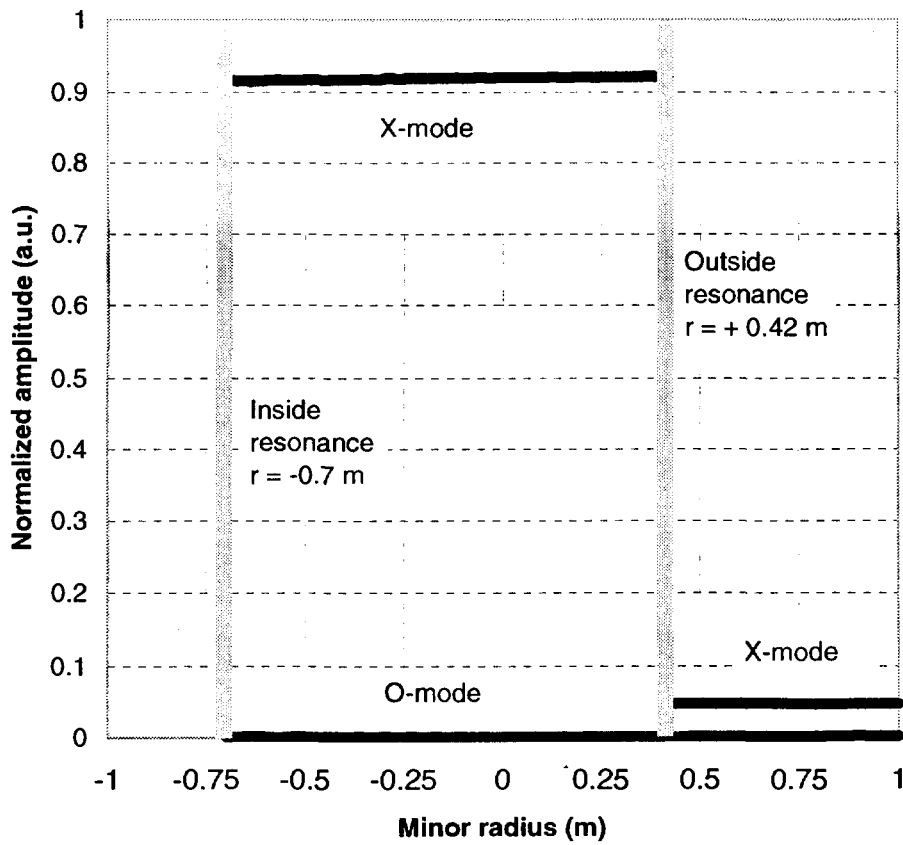


Figure 5b

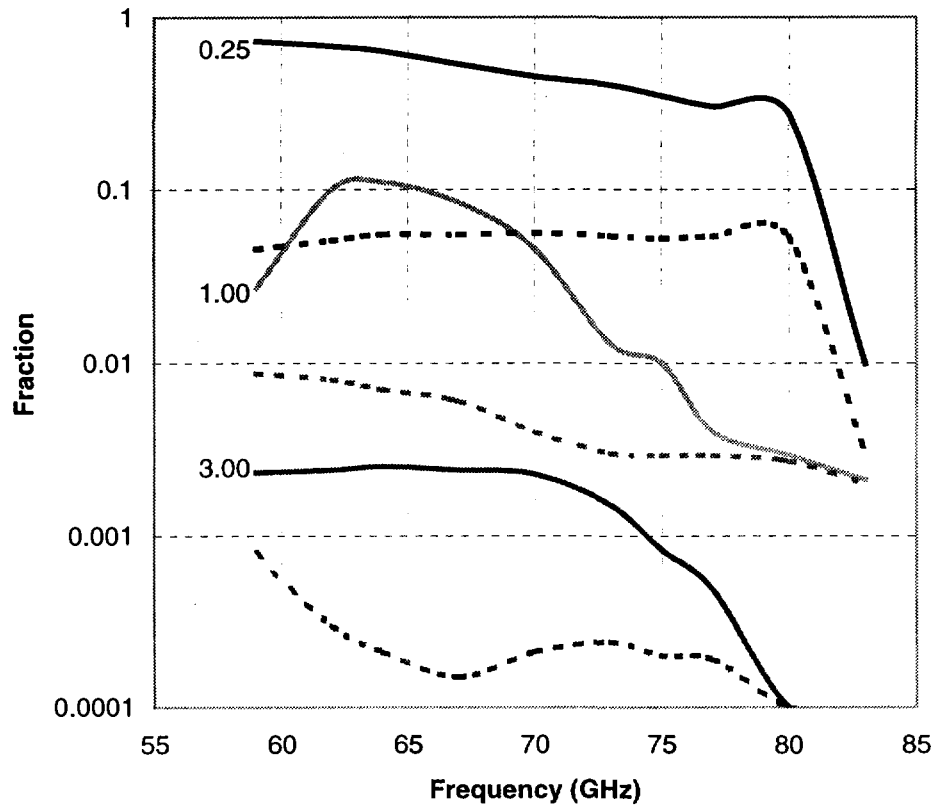


Figure 5c

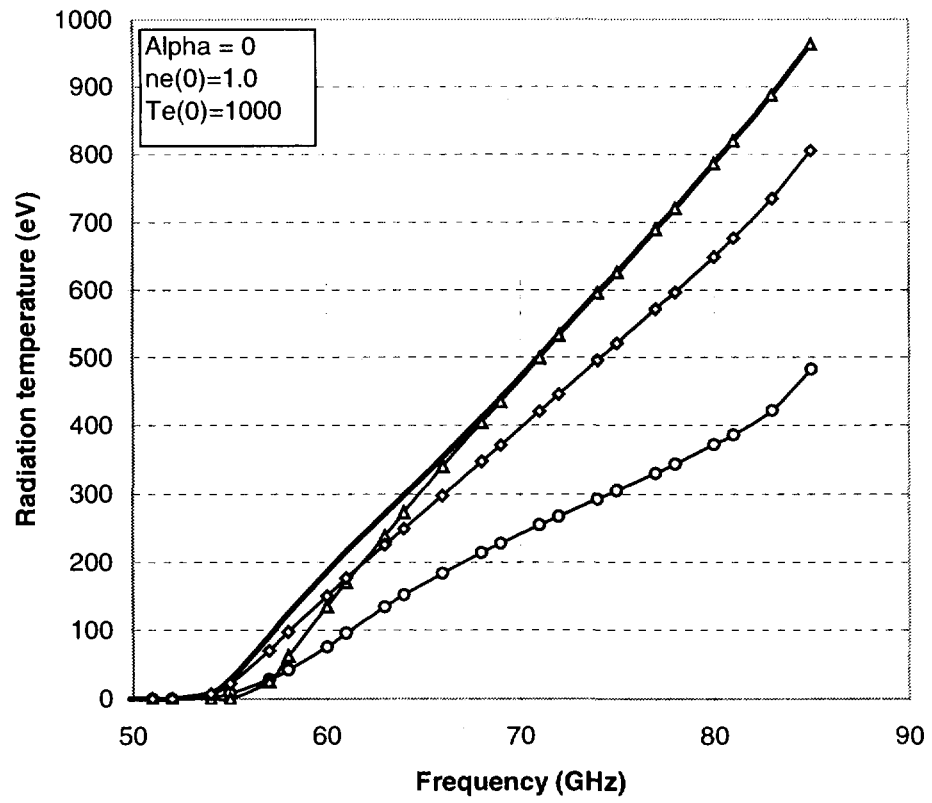


Figure 6



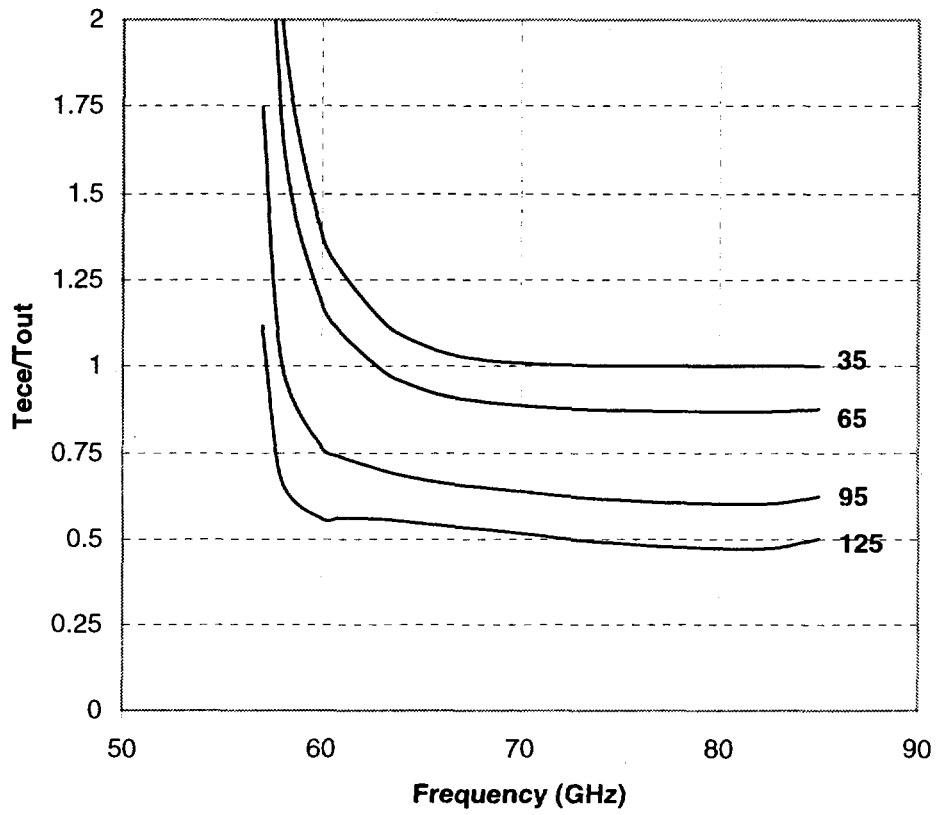


Figure 7a

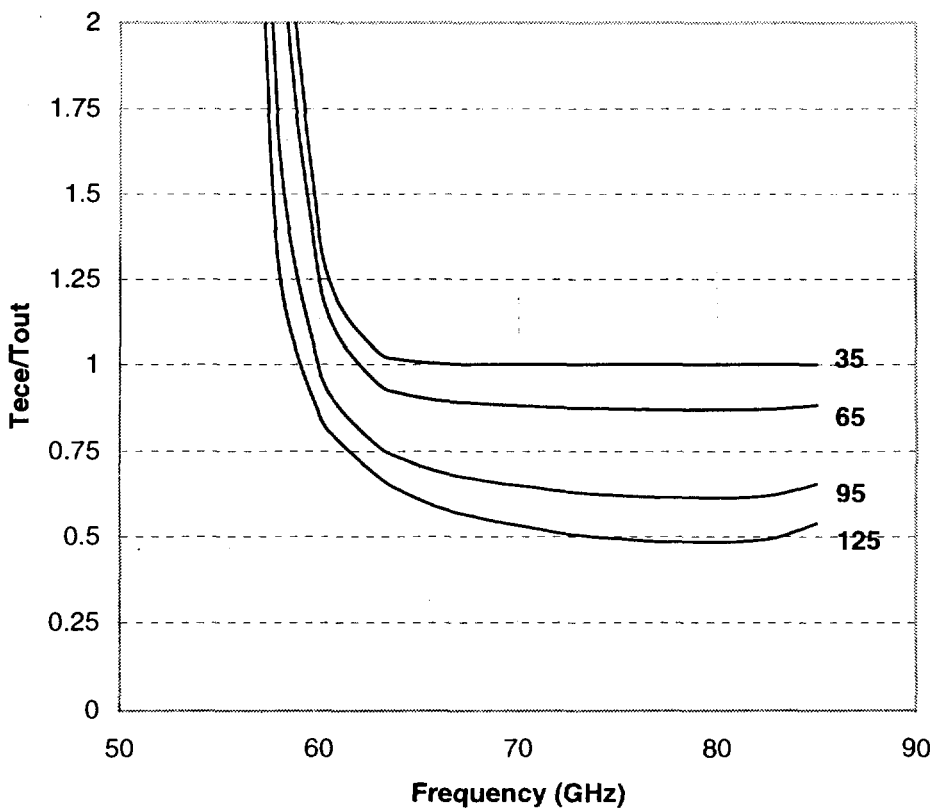


Figure 7b

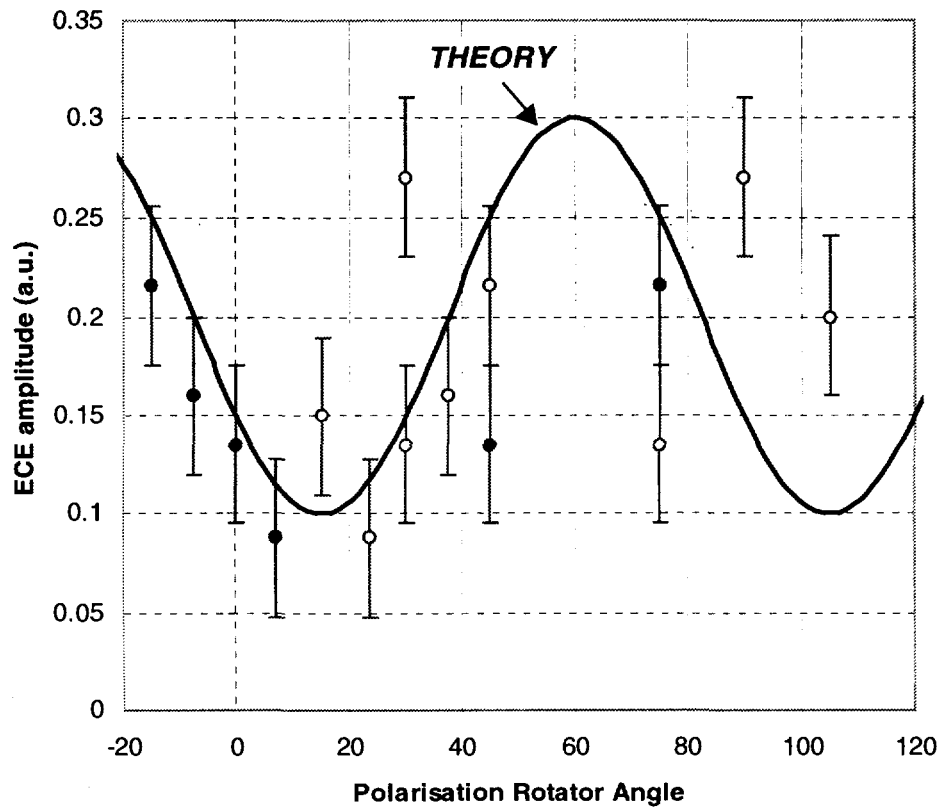


Figure 8

## Recent Issues of NIFS Series

- NIFS-540 H. Nakamura, K. Ikeda and S. Yamaguchi,  
*Transport Coefficients of InSb in a Strong Magnetic Field*; Feb. 1998
- NIFS-541 J. Uramoto,  
*Development of  $\nu_\mu$  Beam Detector and Large Area  $\nu_\mu$  Beam Source by  $H_2$  Gas Discharge (I)*; Mar. 1998
- NIFS-542 J. Uramoto,  
*Development of  $\bar{\nu}_\mu$  Beam Detector and Large Area  $\bar{\nu}_\mu$  Beam Source by  $H_2$  Gas Discharge (II)*;  
Mar. 1998
- NIFS-543 J. Uramoto,  
*Some Problems inside a Mass Analyzer for Pions Extracted from a  $H_2$  Gas Discharge*; Mar. 1998
- NIFS-544 J. Uramoto,  
*Simplified  $\nu_\mu$   $\bar{\nu}_\mu$  Beam Detector and  $\nu_\mu$   $\bar{\nu}_\mu$  Beam Source by Interaction between an Electron Bunch and a Positive Ion Bunch*; Mar. 1998
- NIFS-545 J. Uramoto,  
*Various Neutrino Beams Generated by  $D_2$  Gas Discharge*; Mar. 1998
- NIFS-546 R. Kanno, N. Nakajima, T. Hayashi and M. Okamoto,  
*Computational Study of Three Dimensional Equilibria with the Bootstrap Current*; Mar. 1998
- NIFS-547 R. Kanno, N. Nakajima and M. Okamoto,  
*Electron Heat Transport in a Self-Similar Structure of Magnetic Islands*; Apr. 1998
- NIFS-548 J.E. Rice,  
*Simulated Impurity Transport in LHD from MIST*; May 1998
- NIFS-549 M.M. Skoric, T. Sato, A.M. Maluckov and M.S. Jovanovic,  
*On Kinetic Complexity in a Three-Wave Interaction*; June 1998
- NIFS-550 S. Goto and S. Kida,  
*Passive Saclar Spectrum in Isotropic Turbulence: Prediction by the Lagrangian Direct-interaction Approximation*; June 1998
- NIFS-551 T. Kuroda, H. Sugama, R. Kanno, M. Okamoto and W. Horton,  
*Initial Value Problem of the Toroidal Ion Temperature Gradient Mode* ; June 1998
- NIFS-552 T. Mutoh, R. Kumazawa, T. Seki, F. Simpo, G. Nomura, T. Ido and T. Watari,  
*Steady State Tests of High Voltage Ceramic Feedthroughs and Co-Axial Transmission Line of ICRF Heating System for the Large Helical Device* ; June 1998
- NIFS-553 N. Noda, K. Tsuzuki, A. Sagara, N. Inoue, T. Muroga,  
*Oronization in Future Devices -Protecting Layer against Tritium and Energetic Neutrals-*; July 1998
- NIFS-554 S. Murakami and H. Saleem,  
*Electromagnetic Effects on Rippling Instability and Tokamak Edge Fluctuations*; July 1998
- NIFS-555 H. Nakamura, K. Ikeda and S. Yamaguchi,  
*Physical Model of Nernst Element*; Aug. 1998
- NIFS-556 H. Okumura, S. Yamaguchi, H. Nakamura, K. Ikeda and K. Sawada,  
*Numerical Computation of Thermoelectric and Thermomagnetic Effects*; Aug. 1998
- NIFS-557 Y. Takeiri, M. Osakabe, K. Tsumori, Y. Oka, O. Kaneko, E. Asano, T. Kawamoto, R. Akiyama and M. Tanaka,  
*Development of a High-Current Hydrogen-Negative Ion Source for LHD-NBI System*; Aug. 1998
- NIFS-558 M. Tanaka, A. Yu Grosberg and T. Tanaka,  
*Molecular Dynamics of Structure Organization of Polyampholytes*; Sep. 1998

- NIFS-559 R. Horiuchi, K. Nishimura and T. Watanabe,  
*Kinetic Stabilization of Tilt Disruption in Field-Reversed Configurations*; Sep. 1998  
(IAEA-CN-69/THP1/11)
- NIFS-560 S. Sudo, K. Kholopenkov, K. Matsuoka, S. Okamura, C. Takahashi, R. Akiyama, A. Fujisawa, K. Ida, H. Idei, H. Iguchi, M. Isobe, S. Kado, K. Kondo, S. Kubo, H. Kuramoto, T. Minami, S. Morita, S. Nishimura, M. Osakabe, M. Sasao, B. Peterson, K. Tanaka, K. Toi and Y. Yoshimura,  
*Particle Transport Study with Tracer-Encapsulated Solid Pellet Injection*; Oct. 1998  
(IAEA-CN-69/EXP1/18)
- NIFS-561 A. Fujisawa, H. Iguchi, S. Lee, K. Tanaka, T. Minami, Y. Yoshimura, M. Osakabe, K. Matsuoka, S. Okamura, H. Idei, S. Kubo, S. Ohdachi, S. Morita, R. Akiyama, K. Toi, H. Sanuki, K. Itoh, K. Ida, A. Shimizu, S. Takagi, C. Takahashi, M. Kojima, S. Hidekuma, S. Nishimura, M. Isobe, A. Ejiri, N. Inoue, R. Sakamoto, Y. Hamada and M. Fujiwara,  
*Dynamic Behavior Associated with Electric Field Transitions in CHS Heliotron/Torsatron*; Oct. 1998  
(IAEA-CN-69/EX5/1)
- NIFS-562 S. Yoshikawa,  
*Next Generation Toroidal Devices*; Oct. 1998
- NIFS-563 Y. Todo and T. Sato,  
*Kinetic-Magnetohydrodynamic Simulation Study of Fast Ions and Toroidal Alfvén Eigenmodes*; Oct. 1998  
(IAEA-CN-69/THP2/22)
- NIFS-564 T. Watari, T. Shimozuma, Y. Takeiri, R. Kumazawa, T. Mutoh, M. Sato, O. Kaneko, K. Ohkubo, S. Kubo, H. Idei, Y. Oka, M. Osakabe, T. Seki, K. Tsumori, Y. Yoshimura, R. Akiyama, T. Kawamoto, S. Kobayashi, F. Shimpō, Y. Takita, E. Asano, S. Itoh, G. Nomura, T. Ido, M. Hamabe, M. Fujiwara, A. Iiyoshi, S. Morimoto, T. Bigelow and Y.P. Zhao,  
*Steady State Heating Technology Development for LHD*; Oct. 1998  
(IAEA-CN-69/FTP/21)
- NIFS-565 A. Sagara, K.Y. Watanabe, K. Yamazaki, O. Motojima, M. Fujiwara, O. Mitarai, S. Imagawa, H. Yamanishi, H. Chikaraishi, A. Kohyama, H. Matsui, T. Muroga, T. Noda, N. Ohyabu, T. Satow, A.A. Shishkin, S. Tanaka, T. Terai and T. Uda,  
*LHD-Type Compact Helical Reactors*; Oct. 1998  
(IAEA-CN-69/FTP/03(R))
- NIFS-566 N. Nakajima, J. Chen, K. Ichiguchi and M. Okamoto,  
*Global Mode Analysis of Ideal MHD Modes in  $L=2$  Heliotron/Torsatron Systems*; Oct. 1998  
(IAEA-CN-69/THP1/08)
- NIFS-567 K. Ida, M. Osakabe, K. Tanaka, T. Minami, S. Nishimura, S. Okamura, A. Fujisawa, Y. Yoshimura, S. Kubo, R. Akiyama, D.S.Darrow, H. Idei, H. Iguchi, M. Isobe, S. Kado, T. Kondo, S. Lee, K. Matsuoka, S. Morita, I. Nomura, S. Ohdachi, M. Sasao, A. Shimizu, K. Tsumori, S. Takayama, M. Takechi, S. Takagi, C. Takahashi, K. Toi and T. Watari,  
*Transition from  $L$  Mode to High Ion Temperature Mode in CHS Heliotron/Torsatron Plasmas*; Oct. 1998  
(IAEA-CN-69/EX2/2)
- NIFS-568 S. Okamura, K. Matsuoka, R. Akiyama, D.S. Darrow, A. Ejiri, A. Fujisawa, M. Fujiwara, M. Goto, K. Ida, H. Idei, H. Iguchi, N. Inoue, M. Isobe, K. Itoh, S. Kado, K. Kholopenkov, T. Kondo, S. Kubo, A. Lazaros, S. Lee, G. Matsunaga, T. Minami, S. Morita, S. Murakami, N. Nakajima, N. Nikai, S. Nishimura, I. Nomura, S. Ohdachi, K. Ohkuni, M. Osakabe, R. Pavlichenko, B. Peterson, R. Sakamoto, H. Sanuki, M. Sasao, A. Shimizu, Y. Shirai, S. Sudo, S. Takagi, C. Takahashi, S. Takayama, M. Takechi, K. Tanaka, K. Toi, K. Yamazaki, Y. Yoshimura and T. Watari,  
*Confinement Physics Study in a Small Low-Aspect-Ratio Helical Device CHS*; Oct. 1998  
(IAEA-CN-69/OV4/5)
- NIFS-569 M.M. Skoric, T. Sato, A. Maluckov, M.S. Jovanovic,  
*Micro- and Macro-scale Self-organization in a Dissipative Plasma*; Oct. 1998
- NIFS-570 T. Hayashi, N. Mizuguchi, T-H. Watanabe, T. Sato and the Complexity Simulation Group,  
*Nonlinear Simulations of Internal Reconnection Event in Spherical Tokamak*; Oct. 1998  
(IAEA-CN-69/TH3/3)
- NIFS-571 A. Iiyoshi, A. Komori, A. Ejiri, M. Emoto, H. Funaba, M. Goto, K. Ida, H. Idei, S. Inagaki, S. Kado, O. Kaneko, K. Kawahata, S. Kubo, R. Kumazawa, S. Masuzaki, T. Minami, J. Miyazawa, T. Morisaki, S. Morita, S. Murakami, S. Muto, T. Muto, Y. Nagayama, Y. Nakamura, H. Nakanishi, K. Narihara, K. Nishimura, N. Noda, T. Kobuchi, S. Ohdachi, N. Ohyabu, Y. Oka, M. Osakabe, T. Ozaki, B.J. Peterson, A. Sagara, S. Sakakibara, R. Sakamoto, H. Sasao, M. Sasao, K. Sato, M. Sato, T. Seki, T. Shimozuma, M. Shoji, H. Suzuki, Y. Takeiri, K. Tanaka, K. Toi, T. Tokuzawa, K. Tsumori, I. Yamada, H. Yamada, S. Yamaguchi, M. Yokoyama, K.Y. Watanabe, T. Watari, R. Akiyama, H. Chikaraishi, K. Haba, S. Hamaguchi, S. Iima, S. Imagawa, N. Inoue, K. Iwamoto, S. Kitagawa, Y. Kubota, J. Kodaira, R. Maekawa, T. Mito, T. Nagasaka, A. Nishimura, Y. Takita, C. Takahashi, K. Takahata, K. Yamauchi, H. Tamura, T. Tsuzuki, S. Yamada, N. Yanagi, H. Yonezu, Y. Hamada, K. Matsuoka, K. Murai, K. Ohkubo, I. Ohtake, M. Okamoto, S. Sato, T. Satow, S. Sudo, S. Tanahashi, K. Yamazaki, M. Fujiwara and O. Motojima,  
*An Overview of the Large Helical Device Project*; Oct. 1998  
(IAEA-CN-69/OV1/4)

- NIFS-572 M. Fujiwara, H. Yamada, A. Ejiri, M. Emoto, H. Funaba, M. Goto, K. Ida, H. Idei, S. Inagaki, S. Kado, O. Kaneko, K. Kawahata, A. Komori, S. Kubo, R. Kumazawa, S. Masuzaki, T. Minami, J. Miyazawa, T. Morisaki, S. Morita, S. Murakami, S. Muto, T. Muto, Y. Nagayama, Y. Nakamura, H. Nakanishi, K. Narihara, K. Nishimura, N. Noda, T. Kobuchi, S. Ohdachi, N. Ohyabu, Y. Oka, M. Osakabe, T. Ozaki, B. J. Peterson, A. Sagara, S. Sakakibara, R. Sakamoto, H. Sasao, M. Sasao, K. Sato, M. Sato, T. Seki, T. Shimozuma, M. Shoji, H. Suzuki, Y. Takeiri, K. Tanaka, K. Toi, T. Tokuzawa, K. Tsumori, I. Yamada, S. Yamaguchi, M. Yokoyama, K.Y. Watanabe, T. Watan, R. Akiyama, H. Chikaraishi, K. Haba, S. Hamaguchi, M. Ima, S. Imagawa, N. Inoue, K. Iwamoto, S. Kitagawa, Y. Kubota, J. Kodaira, R. Maekawa, T. Mito, T. Nagasaka, A. Nishimura, Y. Takita, C. Takahashi, K. Takahata, K. Yamauchi, H. Tamura, T. Tsuzuki, S. Yamada, N. Yanagi, H. Yonezu, Y. Hamada, K. Matsuoka, K. Murai, K. Ohkubo, I. Ohtake, M. Okamoto, S. Sato, T. Satow, S. Sudo, S. Tanahashi, K. Yamazaki, O. Motojima and A. Iiyoshi,  
*Plasma Confinement Studies in LHD*; Oct. 1998  
(IAEA-CN-69/EX2/3)
- NIFS-573 O. Motojima, K. Akaishi, H. Chikaraishi, H. Funaba, S. Hamaguchi, S. Imagawa, S. Inagaki, N. Inoue, A. Iwamoto, S. Kitagawa, A. Komori, Y. Kubota, R. Maekawa, S. Masuzaki, T. Mito, J. Miyazawa, T. Morisaki, T. Muroga, T. Nagasaka, Y. Nakamura, A. Nishimura, K. Nishimura, N. Noda, N. Ohyabu, S. Sagara, S. Sakakibara, R. Sakamoto, S. Satoh, T. Satow, M. Shoji, H. Suzuki, K. Takahata, H. Tamura, K. Watanabe, H. Yamada, S. Yamada, S. Yamaguchi, K. Yamazaki, N. Yanagi, T. Baba, H. Hayashi, M. Ima, T. Inoue, S. Kato, T. Kato, T. Kondo, S. Moriuchi, H. Ogawa, I. Ohtake, K. Ooba, H. Sekiguchi, N. Suzuki, S. Takami, Y. Taniguchi, T. Tsuzuki, N. Yamamoto, K. Yasui, H. Yonezu, M. Fujiwara and A. Iiyoshi,  
*Progress Summary of LHD Engineering Design and Construction*; Oct. 1998  
(IAEA-CN-69/FT2/1)
- NIFS-574 K. Toi, M. Takechi, S. Takagi, G. Matsunaga, M. Isobe, T. Kondo, M. Sasao, D.S. Darrow, K. Ohkuni, S. Ohdachi, R. Akiyama, A. Fujisawa, M. Gotoh, H. Idei, K. Ida, H. Iguchi, S. Kado, M. Kojima, S. Kubo, S. Lee, K. Matsuoka, T. Minami, S. Morita, N. Nikai, S. Nishimura, S. Okamura, M. Osakabe, A. Shimizu, Y. Shirai, C. Takahashi, K. Tanaka, T. Watan and Y. Yoshimura,  
*Global MHD Modes Excited by Energetic Ions in Heliotron/Torsatron Plasmas*; Oct. 1998  
(IAEA-CN-69/EXP1/19)
- NIFS-575 Y. Hamada, A. Nishizawa, Y. Kawasumi, A. Fujisawa, M. Kojima, K. Narihara, K. Ida, A. Ejiri, S. Ohdachi, K. Kawahata, K. Toi, K. Sato, T. Seki, H. Iguchi, K. Adachi, S. Hidekuma, S. Hirokura, K. Iwasaki, T. Ido, R. Kumazawa, H. Kuramoto, T. Minami, I. Nomura, M. Sasao, K.N. Sato, T. Tsuzuki, I. Yamada and T. Watari,  
*Potential Turbulence in Tokamak Plasmas*; Oct. 1998  
(IAEA-CN-69/EXP2/14)
- NIFS-576 S. Murakami, U. Gasparino, H. Idei, S. Kubo, H. Maassberg, N. Marushchenko, N. Nakajima, M. Romé and M. Okamoto,  
*5D Simulation Study of Suprathermal Electron Transport in Non-Axisymmetric Plasmas*; Oct. 1998  
(IAEA-CN-69/THP1/01)
- NIFS-577 S. Fujiwara and T. Sato,  
*Molecular Dynamics Simulation of Structure Formation of Short Chain Molecules*; Nov. 1998
- NIFS-578 T. Yamagishi,  
*Eigenfunctions for Vlasov Equation in Multi-species Plasmas* Nov. 1998
- NIFS-579 M. Tanaka, A. Yu Grosberg and T. Tanaka,  
*Molecular Dynamics of Strongly-Coupled Multichain Coulomb Polymers in Pure and Salt Aqueous Solutions*; Nov. 1998
- NIFS-580 J. Chen, N. Nakajima and M. Okamoto,  
*Global Mode Analysis of Ideal MHD Modes in a Heliotron/Torsatron System: I. Mercier-unstable Equilibria*; Dec. 1998
- NIFS-581 M. Tanaka, A. Yu Grosberg and T. Tanaka,  
*Comparison of Multichain Coulomb Polymers in Isolated and Periodic Systems: Molecular Dynamics Study*; Jan. 1999
- NIFS-582 V.S. Chan and S. Murakami,  
*Self-Consistent Electric Field Effect on Electron Transport of ECH Plasmas*; Feb. 1999
- NIFS-583 M. Yokoyama, N. Nakajima, M. Okamoto, Y. Nakamura and M. Wakatani,  
*Roles of Bumpy Field on Collisionless Particle Confinement in Helical-Axis Heliotrons*; Feb. 1999
- NIFS-584 T.-H. Watanabe, T. Hayashi, T. Sato, M. Yamada and H. Ji,  
*Modeling of Magnetic Island Formation in Magnetic Reconnection Experiment*; Feb. 1999
- NIFS-585 R. Kumazawa, T. Mutoh, T. Seki, F. Shinpo, G. Nomura, T. Ido, T. Watari, Jean-Marie Noterdaeme and Yangping Zhao,  
*Liquid Stub Tuner for Ion Cyclotron Heating*; Mar. 1999
- NIFS-586 A. Sagara, M. Ima, S. Inagaki, N. Inoue, H. Suzuki, K. Tsuzuki, S. Masuzaki, J. Miyazawa, S. Morita, Y. Nakamura, N. Noda, B. Peterson, S. Sakakibara, T. Shimozuma, H. Yamada, K. Akaishi, H. Chikaraishi, H. Funaba, O. Kaneko, K. Kawahata, A. Komori,

- N. Ohyaibu, O. Motojima, LHD Exp. Group 1, LHD Exp. Group 2,  
*Wall Conditioning at the Starting Phase of LHD*; Mar. 1999
- NIFS-587 T. Nakamura and T. Yabe,  
*Cubic Interpolated Propagation Scheme for Solving the Hyper-Dimensional Vlasov-Poisson Equation in Phase Space*; Mar. 1999
- NIFS-588 W.X. Wnag, N. Nakajima, S. Murakami and M. Okamoto,  
*An Accurate  $\delta f$  Method for Neoclassical Transport Calculation* ;Mar. 1999
- NIFS-589 K. Kishida, K. Araki, S. Kishiba and K. Suzuki,  
*Local or Nonlocal? Orthonormal Divergence-free Wavelet Analysis of Nonlinear Interactions in Turbulence*; Mar. 1999
- NIFS-590 K. Araki, K. Suzuki, K. Kishida and S. Kishiba,  
*Multiresolution Approximation of the Vector Fields on  $T^3$* ; Mar. 1999
- NIFS-591 K. Yamazaki, H. Yamada, K.Y. Watanabe, K. Nishimura, S. Yamaguchi, H. Nakanishi, A. Komori, H. Suzuki, T. Mito, H. Chikaraishi, K. Murai, O. Motojima and the LHD Group,  
*Overview of the Large Helical Device (LHD) Control System and Its First Operation*; Apr. 1999
- NIFS-592 T. Takahashi and Y. Nakao,  
*Thermonuclear Reactivity of D-T Fusion Plasma with Spin-Polarized Fuel*; Apr. 1999
- NIFS-593 H. Sugama,  
*Damping of Toroidal Ion Temperature Gradient Modes*; Apr. 1999
- NIFS-594 Xiaodong Li ,  
*Analysis of Crowbar Action of High Voltage DC Power Supply in the LHD ICRF System*; Apr. 1999
- NIFS-595 K. Nishimura, R. Horiuchi and T. Sato,  
*Drift-kink Instability Induced by Beam Ions in Field-reversed Configurations*; Apr. 1999
- NIFS-596 Y. Suzuki, T-H. Watanabe, T. Sato and T. Hayashi,  
*Three-dimensional Simulation Study of Compact Toroid Plasmoid Injection into Magnetized Plasmas*; Apr. 1999
- NIFS-597 H. Sanuki, K. Itoh, M. Yokoyama, A. Fujisawa, K. Ida, S. Toda, S.-I. Itoh, M. Yagi and A. Fukuyama,  
*Possibility of Internal Transport Barrier Formation and Electric Field Bifurcation in LHD Plasma*; May 1999
- NIFS-598 S. Nakazawa, N. Nakajima, M. Okamoto and N. Ohyaibu,  
*One Dimensional Simulation on Stability of Detached Plasma in a Tokamak Divertor*; June 1999
- NIFS-599 S. Murakami, N. Nakajima, M. Okamoto and J. Nhrenberg,  
*Effect of Energetic Ion Loss on ICRF Heating Efficiency and Energy Confinement Time in Heliotrons*; June 1999
- NIFS-600 R. Horiuchi and T. Sato,  
*Three-Dimensional Particle Simulation of Plasma Instabilities and Collisionless Reconnection in a Current Sheet*; June 1999
- NIFS-601 W. Wang, M. Okamoto, N. Nakajima and S. Murakami,  
*Collisional Transport in a Plasma with Steep Gradients*; June 1999
- NIFS-602 T. Mutoh, R. Kurnazawa, T. Saki, K. Saito, F. Simpo, G. Nomura, T. Watari, X. Jikang, G. Cattanei, H. Okada, K. Ohkubo, M. Sato, S. Kubo, T. Shimozuma, H. Idei, Y. Yoshimura, O. Kaneko, Y. Takeiri, M. Osakabe, Y. Oka, K. Tsumori, A. Komori, H. Yamada, K. Watanabe, S. Sakakibara, M. Shoji, R. Sakamoto, S. Inagaki, J. Miyazawa, S. Morita, K. Tanaka, B.J. Peterson, S. Murakami, T. Minami, S. Ohdachi, S. Kado, K. Narihara, H. Sasao, H. Suzuki, K. Kawahata, N. Ohyaibu, Y. Nakamura, H. Funaba, S. Masuzaki, S. Muto, K. Sato, T. Morisaki, S. Sudo, Y. Nagayama, T. Watanabe, M. Sasao, K. Ida, N. Noda, K. Yamazaki, K. Akaishi, A. Sagara, K. Nishimura, T. Ozaki, K. Toi, O. Motojima, M. Fujiwara, A. Iiyoshi and LHD Exp. Group 1 and 2,  
*First ICRF Heating Experiment in the Large Helical Device*; July 1999
- NIFS-603 P.C. de Vries, Y. Nagayama, K. Kawahata, S. Inagaki, H. Sasao and K. Nagasaki,  
*Polarization of Electron Cyclotron Emission Spectra in LHD*; July 1999